Journal of
Synchrotron
Radiation

ISSN 0909-0495

Received 23 February 2004
Accepted 22 October 2004

Mo *K*- and *L*-edge X-ray absorption spectroscopic study of the ADP·AlF_4^--stabilized nitrogenase complex: comparison with MoFe protein in solution and single crystal

Mary C. Corbett,[a] F. Akif Tezcan,[b] Oliver Einsle,[b,c]‡ Mika Y. Walton,[b,c] Douglas C. Rees,[b,c] Matthew J. Latimer,[d] Britt Hedman[d]* and Keith O. Hodgson[a,d]

[a]Department of Chemistry, Stanford University, Stanford, CA 94305, USA, [b]Division of Chemistry and Chemical Engineering, California Institute of Technology, Mail Code 114-96, Pasadena, CA 91125, USA, [c]Howard Hughes Medical Institute, California Institute of Technology, Mail Code 114-96, Pasadena, CA 91125, USA, and [d]Stanford Synchrotron Radiation Laboratory, Stanford University, SLAC, 2575 Sand Hill Road, MS 69, Menlo Park, CA 94025, USA.
E-mail: hedman@ssrl.slac.stanford.edu

The utility of using X-ray absorption spectroscopy (XAS) to study metalloproteins and, specifically, the enzyme complex nitrogenase, is highlighted by this study comparing both the structural and Mo-localized electronic features of the iron–molybdenum cofactor (FeMoco) in isolated MoFe protein and in the ADP·AlF_4^--stabilized complex of the MoFe protein with the Fe protein. No major differences are found at Mo between the two protein forms. The excellent quality of the data at both the Mo *K* and *L* edges will provide a baseline for analysis of other intermediates in the nitrogenase cycle. A new capability to delineate various contributions in the resting state of FeMoco is being pursued through polarized single-crystal XAS. The initial results point to the feasibility of using this technique for the analysis of scattering from the as yet unidentified atom at the center of FeMoco.

Keywords: nitrogenase; EXAFS; XAS; diffraction.

1. Introduction

Nitrogen fixation is catalyzed by the nitrogenase enzyme system (reviewed by Burgess & Lowe, 1996; Howard & Rees, 1996; Smith, 1999; Christiansen *et al.*, 2001; Igarashi & Seefeldt, 2003) according to the following general reaction,

$$N_2 + 8H^+ + 8e^- + 16\text{MgATP} \longrightarrow 2NH_3 + H_2 + 16\text{MgADP} + 16P_i.$$

Nitrogenase is composed of the Fe protein, a homodimer that contains one nucleotide binding site per subunit and a single [4Fe–4S] cluster at the dimer interface, and the MoFe protein, an $\alpha_2\beta_2$ heterotetramer that contains two unique metalloclusters, the [8Fe–7S] P-cluster and FeMoco, a [Mo–7Fe–9S–X]-homocitrate iron–molybdenum cofactor (Fig. 1). Catalysis is believed to occur at FeMoco following nucleotide-dependent electron transfer from the Fe protein. In the kinetic scheme proposed by Thorneley & Lowe (1983, 1985), the [4Fe–4S] cluster in the Fe protein cycles between the 1+ and 2+ redox states as it sequentially transfers electrons to the

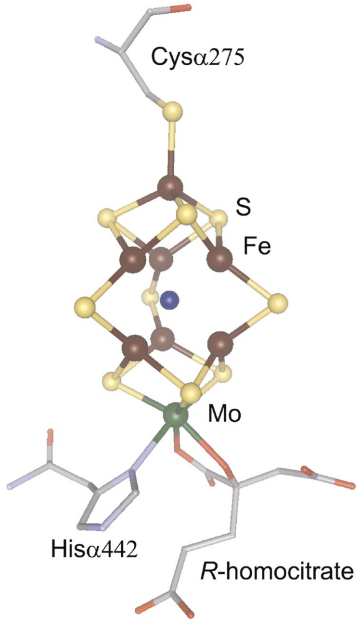

Figure 1
A structural model of FeMoco created from the deposited coordinates of the 1.16 Å resolution MoFe protein crystal structure (PDB 1M1N). The identity of the atom at the cluster center is still unknown but believed to be N, O or C (Einsle *et al.*, 2002).

‡ Current Address: Abteilung für Molekulare Strukturbiologie, Institut für Mikrobiologie und Genetik, Georg-August-Universität Göttingen, Justus-von-Liebig-Weg 11, 37077 Göttingen, Germany.

MoFe protein during a series of rate-limiting component protein–protein complex formation and dissociation reactions. Binding and hydrolysis of MgATP by the Fe protein occur concomitant with each complex formation–dissociation step. Unlike similar nucleotide binding proteins, the Fe protein cannot hydrolyze ATP in the absence of its complex component, the MoFe protein. If one electron is transferred per Fe protein cycle, then eight such cycles are needed to reduce one N_2 molecule. The Fe protein can be reduced *in vitro* to the all-ferrous state, raising the possibility that two electrons may be transferred per cycle instead of one, although the low reduction potential could preclude accessing this state *in vivo* (Angove *et al.*, 1997; Guo *et al.*, 2002). Either way, the requirement for multiple electrons suggests that electrons are transferred to the MoFe protein and then stored, perhaps at the P-cluster, before substrate reduction occurs.

To better understand the roles of the component protein interaction and nucleotide hydrolysis in electron transfer and substrate reduction, the ADP·AlF_4^--stabilized Fe protein–MoFe protein complex has been studied (Duyvis *et al.*, 1996; Renner & Howard, 1996). Aluminium fluoride is widely used as a γ-phosphate mimic to study the transition state of nucleotide hydrolysis (Wittinghofer, 1997). Because ATP hydrolysis only occurs in the complex between the Fe protein and the MoFe protein, treatment of the component proteins together with MgADP and AlF_4^- stabilizes this complex. The *Azotobacter vinelandii* stabilized nitrogenase complex is not active in acetylene reduction or hydrogen evolution, which presumably indicates that FeMoco is not in a state that mimics turnover conditions (Duyvis *et al.*, 1996; Renner & Howard, 1996; Yousafzai & Eady, 1999). Obligate hydrogen evolution, a process requiring two electrons, has been shown to occur, however, in the *Klebsiella pneumoniae* ADP·AlF_4^--stabilized nitrogenase complex and in a tight complex of *Azotobacter vinelandii* MoFe protein with *Clostridium pasteurianum* Fe protein (Clarke *et al.*, 2000; Miller *et al.*, 2001). EPR studies on both *A. vinelandii* and *K. pneumoniae* ADP·AlF_4^--stabilized complexes did not show a major change in the electronic properties of FeMoco in the complex from that of the resting state, although the Fe protein and the P-cluster were shown to be in one-electron oxidized states (Spee *et al.*, 1998; Miller *et al.*, 2001).

Crystallography on the *A. vinelandii* stabilized nitrogenase complex was instrumental in identifying a putative electron transfer pathway, stretching from the [4Fe–4S] center of the Fe protein through the P-cluster to FeMoco (Schindelin *et al.*, 1997; Schmid *et al.*, 2002). However, the resolution of the three-dimensional structure at 2.3 Å is such that small changes in the FeMoco structure would not be observed. A theoretical analysis of potential electron transfer pathways in MoFe protein using the program *HARLEM* identified the Mo-bound homocitrate on FeMoco as the favored end point of electron transfer from the P-cluster to FeMoco (Igarashi & Seefeldt, 2003), which suggests that changes may be taking place at the Mo site of FeMoco in the nitrogenase complex that have not yet been observed. Here we present a detailed comparison of the electronic and structural properties of the Mo site in the ADP·AlF_4^--stabilized nitrogenase complex and isolated FeMoco through Mo-*K* and Mo-*L* X-ray absorption spectroscopy (XAS) edge studies and *K*-edge extended fine-structure (EXAFS) analyses. Additionally, we provide a comparison of the edge and EXAFS features of the MoFe protein in solution and in an oriented single crystal.

2. Experimental

2.1. Protein sample preparation

Azotobacter vinelandii MoFe protein and Fe protein were isolated and purified according to published protocols (Wolle *et al.*, 1992) and kept under rigorously anaerobic conditions. Isolated MoFe protein was prepared in 50 m*M* tris(hydroxymethyl)aminomethane hydrochloride buffer (Tris-HCl) (pH 7.7) containing 200 m*M* NaCl and $Na_2S_2O_4$. The ADP·AlF_4^- complex was prepared by mixing MoFe protein with a sixfold excess of Fe protein in a 50 m*M* Tris-HCl and 100 m*M* 3-(4-morpholino)propane sulfonic acid (MOPS) (pH 7.3) solution containing 100 m*M* NaCl, 6 m*M* NaF, 0.25 m*M* $AlCl_3$, 6 m*M* $MgCl_2$, 5 m*M* Na_2ATP, 15 m*M* phosphocreatine, 0.1 mg ml^{-1} creatine phosphokinase and 5 m*M* $Na_2S_2O_4$. The reaction was run overnight to ensure complete complex formation. The ADP·AlF_4^- complex was separated from unreacted Fe protein by gel-filtration on a Superdex S200 column. The XAS samples were prepared by several concentration and dilution cycles with an Amicon stirred cell (YM50 membrane) using the aforementioned buffers. Following complex formation and concentration, 35% glycerol was added to the buffer for the ADP·AlF_4^- complex as a glassing agent. The final protein concentrations in the EXAFS samples were $\sim$300 mg ml^{-1} or $\sim$2.6 m*M* in Mo for the Av1 isolate and $\sim$200 mg ml^{-1} or $\sim$1.1 m*M* in Mo for the complex.

MoFe protein crystals were obtained using sitting-drop vapor diffusion under anaerobic conditions. The protein solution was 20–30 mg ml^{-1} in 50 m*M* Tris-HCl (pH 8.0) with 200 m*M* NaCl. 13% polyethylene glycol 8000 (PEG) in 0.1 *M* Tris-HCl (pH 8.0) and 0.9 *M* NaCl was used as the precipitant. Crystals appeared overnight and were allowed to grow for several weeks, at which point they were exchanged into 20% 2-methyl-2,4-pentanediol for cryoprotection, mounted on size-16 Hamilton pins with nylon loops, and frozen in liquid N_2.

The protein solution samples were frozen in liquid N_2 and shipped over dry ice. After arrival at the Stanford Synchrotron Radiation Laboratory (SSRL), the samples were gently thawed in sealed vials under continuous Ar purge in an anaerobic chamber. The chamber was taken into a Vacuum Atmospheres inert-atmosphere (N_2) dry glovebox prior to opening. For *L*-edge experiments the proteins were transferred by syringe into sealed XAS cryostat cells with 6.25 µm polypropylene windows and maintained at 277 K in a He-purged atmosphere throughout data collection. For *K*-edge experiments, the proteins were transferred by syringe into nylon XAS cells, which were then sealed. The cells were flash frozen in liquid N_2 immediately following removal from the glovebox and stored at 77 K until data collection.

2.2. XAS data collection

All X-ray absorption data were collected at SSRL under normal conditions (3.0 GeV, 60–100 mA). The Mo *L*-edge spectra were measured using the 54-pole wiggler beamline 6-2, in high-field mode with a Ni-coated harmonic rejection mirror and a fully tuned Si(111) double-crystal monochromator. A detailed description of the experimental set-up has been previously published (Hedman *et al.*, 1988). The X-ray energy was calibrated to the maximum in the first pre-edge feature of the S *K*-edge spectrum of $Na_2S_2O_3{\cdot}5H_2O$ set at 2472.02 eV. Powder samples of $Na_2S_2O_3{\cdot}5H_2O$ were run before and after data collection. The data were measured as fluorescence using a N_2-filled Lytle ionization chamber detector over the energy range 2450–2810 eV, which includes the S-*K*, Mo-L_3 and Mo-L_2 edges. An energy step of 0.1 eV was used over the edge regions, with a step of 0.5 eV in the interim and a maximum step size of 4 eV over the post-edge.

The solution Mo *K*-edge spectra were measured using the unfocused eight-pole 1.8 T wiggler beamline 7-3, using a Si(220) double-crystal monochromator, which was detuned by 25% to minimize the presence of harmonic components. During data collection, the samples were maintained at 10 K in an Oxford Instruments CF1208 continuous-flow liquid-He cryostat. Data were collected as Mo $K\alpha$ fluorescence using a Canberra 30-element solid-state Ge detector. The X-ray energy was calibrated to the inflection point at 20003.9 eV of a standard Mo foil measured concurrent with the protein samples between two ionization chambers in line with the cryostat. For the isolated MoFe protein, 15 scans to a *k* value of 18 Å^{-1} and 16 scans to a *k* value of 22 Å^{-1} were collected; 28 scans to a *k* value of 18 Å^{-1} were collected for the nitrogenase complex.

The single-crystal Mo *K*-edge spectra were measured using the 16-pole, 2.0 T wiggler beamline 9-3, with a fully tuned Si(220) double-crystal monochromator, and two Rh-coated mirrors, one flat pre-monochromator mirror for harmonic rejection and vertical collimation, and one toroidal post-monochromator mirror for vertical and horizontal focusing. A detailed description of the single-crystal XAS beamline is found in a separate article in this issue (Latimer *et al.*, 2005). The protein crystal, which was approximately cubic in shape and measured ~500 µm in each direction, was mounted on a Huber Kappa goniometer and maintained at 108 K with an Oxford Instruments liquid-N_2 cryostream. XAS data were measured and calibrated as described above for solution samples. 20 scans to a *k* value of 18 Å^{-1} were collected.

2.3. X-ray diffraction data collection and unit-cell determination

X-ray diffraction data were measured at 0.992 Å (12300 eV) with a Mar Research CCD 165 detector on beamline 9-3 in the configuration described above. 5 s exposures about a 1° φ-rotation at three different κ and ω angles were collected prior to the start of the XAS experiment. Using the program *MOSFLM* (version 6.2.1) (Leslie, 1992), the crystal was determined to have $P2_1$ symmetry with unit-cell dimensions of a = 80.1 Å, b = 130.2 Å, c = 108.1 Å, β = 111.0°. This crystal form is known to contain one molecule in the asymmetric unit (Kim & Rees, 1992).

2.4. XAS data analysis

The energy scales of the Mo *L*-edge spectra were internally calibrated by aligning the first pre-edge peak at ~2474.2 eV of the S *K* edge of $S_2O_4^{2-}$, which was present as an oxygen scavenger in both protein samples, and which was externally calibrated to $S_2O_3^{2-}$ as described above. The S *K* edge was normalized to an edge jump of 1.0 at 2510 eV. As the S EXAFS underlie the Mo *L* edge, a conventional pre-edge subtraction and normalization of the data was not feasible. Following the procedure of George *et al.* (1990) and using the program suite *EXAFSPAK* (George, 1990), the background structure in the Mo *L* edge was approximated by fitting two cubic polynomials in 10 eV intervals over a 20 eV segment centered at the edge. The polynomial intervals were extrapolated through the edge region and constrained to join smoothly. This cubic spline was then subtracted from the data, to give the resulting Mo *L*-edge spectra.

The Mo *K*-edge data were normalized using the program *XFIT* (Ellis & Freeman, 1995) by first subtracting a linear background absorbance that was fit to the pre-edge region and extended over the post-edge, followed by fitting a four-segment polynomial spline over the EXAFS region, and finally by normalizing the resulting absorbance spectra to an edge jump of 1.0 at 20020 eV. The EXAFS data between *k* values of 2 Å^{-1} and 18 Å^{-1} were fit using *EXAFSPAK* (George, 1990) to *ab initio* theoretical phase and amplitude functions generated by *FEFF* (version 7.0) (Mustre de Leon *et al.*, 1991; Rehr & Albers, 2000) from the coordinates of FeMoco in the 1.16 Å-resolution MoFe protein crystal structure [PDB file 1M1N (Einsle *et al.*, 2002)].

3. Results and discussion

3.1. Nitrogenase complex structural results

Previous EXAFS studies on isolated MoFe protein demonstrated that the Mo *K*-edge EXAFS spectrum is sensitive to the long-range order in the cluster of the FeMo cofactor (Liu *et al.*, 1994). Specifically, these studies identified a peak in the EXAFS Fourier transform at ~4.8 Å corresponding to Mo–Fe scattering, which should be drastically affected by a loss of symmetry in the cluster. Therefore, a comparison of the EXAFS data (Fig. 2) and EXAFS fitting results (Table 1) for the isolated MoFe protein and the ADP·AlF_4^--stabilized nitrogenase complex would highlight even subtle changes in the FeMoco structure if any occurred upon complex formation. Accounting for the noise level of the data, there does not appear to be any difference in the structure of these two species. The spectra and the fit parameters are almost identical except for a slight increase in the disorder associated with the 5.09 Å Fe–Fe scattering interaction in the nitrogenase complex, attributable to the poorer data quality of this sample. The absence of any change to the

Table 1
Mo *K*-edge EXAFS fitting results for the ADP·AlF_4^--stabilized nitrogenase complex and isolated MoFe protein in solution and single crystal.

The average crystallographically determined distances from Mo in the MoFe protein, based on the deposited coordinates of the 1.16 Å structure, are: O/N at 2.22 ± 0.06 Å, S at 2.34 ± 0.02 Å, Fe at 2.69 ± 0.03 Å and 5.06 ± 0.03 Å. The variables are coordination number, *N*; interatomic distance, *R*; mean-square thermal and static deviation in *R*, σ^2; and the shift in the threshold energy, ΔE_0. *R*, σ^2 and ΔE_0 were allowed to float during the fitting process; a single ΔE_0 was used for each fit. The estimated uncertainties in *R* and σ^2 are 0.02 Å and 0.0001 $Å^2$, respectively. Error is reported as $[\Sigma k^6(\chi_{exptl} - \chi_{calcd})^2]/n$ where *n* is the number of data points.

	Mo—O/N			Mo—S			Mo—Fe			Mo—Fe				
	N	*R* (Å)	σ^2 ($Å^2$)	*N*	*R* (Å)	σ^2 ($Å^2$)	*N*	*R* (Å)	σ^2 ($Å^2$)	*N*	*R* (Å)	σ^2 ($Å^2$)	ΔE_0 (eV)	Error
MoFe protein (solution) k = 2–18 $Å^{-1}$	3	2.21	0.0031	3	2.37	0.0022	3	2.70	0.0029	3	5.09	0.0038	−7.6	0.43
AlF_4^- complex (solution) k = 2–18 $Å^{-1}$	3	2.21	0.0030	3	2.37	0.0024	3	2.70	0.0030	3	5.09	0.0047	−7.4	1.32
MoFe protein (crystal) k = 2–17.2 $Å^{-1}$	3	2.24	0.0014	3	2.36	0.0028	3	2.70	0.0029	3	5.09	0.0042	−3.9	1.00

Mo EXAFS in the putative transition-state complex provides structural evidence that the FeMoco cluster is not deformed at this stage in the enzyme cycle.

3.2. Nitrogenase complex electronic results

To assess the electronic state of the Mo center in FeMoco, the L_3- and L_2-edge spectra were recorded. These edges probe transitions from the $2p_{3/2}$ and $2p_{1/2}$ initial states. The 'white line' feature arises from a $2p \rightarrow 4d$ transition (Hedman *et al.*, 1984). This feature is composed of two components, previously assigned in isolated FeMoco as α and β, which are due to ligand field splitting of the Mo 4*d* orbitals and, therefore, provide a means of probing changes in the symmetry about Mo (Hedman *et al.*, 1988). The Mo *L* edge has been shown to be sensitive to the oxidation state of the Mo center, exhibiting an ∼3 eV range across the Mo oxidation states +4 through +6 for octahedral complexes, and is also sensitive to changes in ligation (Hedman *et al.*, 1984; George *et al.*, 1990). The Mo *K* edge, which probes transitions from the 1*s* orbital, is also sensitive to electronic changes at the Mo center, but the edge features are broadened by the extended core-hole lifetime and the decreased monochromator resolution at this energy, limiting the scope of analysis (Hedman *et al.*, 1984).

Fig. 3 displays the Mo L_3 and L_2 edges, with the associated second derivatives, of isolated MoFe protein and the ADP·AlF_4^--stabilized nitrogenase complex. The Mo *L* edge lies ∼50 eV above the S *K* edge in energy, leading to complications in the *L*-edge background from S EXAFS features. The differing S environments and concentrations in these proteins make background subtraction and normalization at the Mo *L* edge difficult. Therefore, the intensities of the *L* edges displayed here are not quantitative and the intensity differences seen in these spectra are not accurate. Unaffected, and of particular relevance, however, is the similarity in the splitting and position of the 'white line' features in these proteins, exemplified by the correlation in their second derivatives. The MoFe proteins in both the as-isolated and the stabilized complex states have similar Mo edge features within the noise level of the data. This result indicates a lack of electronic, ligation or major geometric change at the Mo center upon complex formation. The Mo *K* edges shown in Fig. 4 further support this conclusion, as they are also identical, within the experimental limits, for isolated and complexed MoFe protein.

The analyses presented here provide an extremely sensitive probe of differences in the order and local structure of FeMoco and the electronic environment of the Mo atom in FeMoco between isolated MoFe protein and the nitrogenase complex. Taken together, the *K*-edge EXAFS and the *L*-edge structure comparisons indicate that the FeMoco cluster is not perturbed from the perspective of Mo in the ADP·AlF_4^--stabilized nitrogenase complex. This study would not be sensitive to electronic changes at Fe, nor to slight structural changes at the Fe sites, such as the binding of a light atom that would not lead to changes in the interatomic Mo—Fe distances or order in the cluster. Therefore, the conclusions presented here, while in agreement with previous structural, biochemical and EPR results (Duyvis *et al.*, 1996; Schindelin *et al.*, 1997; Spee *et al.*, 1998) and the Thorneley–Lowe kinetic scheme, which does not predict activity at the FeMoco center until several cycles of Fe protein complexation have occurred (Thorneley & Lowe, 1985), do not completely eliminate the possibility that some minor change has occurred at Fe in FeMoco in the ADP·AlF_4^--stabilized complex. A lack of change in the Mo environment of FeMoco in the complex strongly implies that minimal change has occurred at FeMoco and, therefore, raises questions as to how the MoFe protein and its metalloclusters are affected by the cycle of complex formation and electron transfer. If FeMoco is indeed the site of substrate reduction and the ultimate acceptor of the transferred electrons, as it is believed to be, the study of the Mo *K*- and *L*-edge properties detailed here will provide a necessary background for evaluating the changes that take place at this center in a protein representative of a more advanced transition state, assuming that such changes are large enough to affect the Mo site.

3.3. MoFe protein solution *versus* single-crystal data

The recent discovery of a central atom in the FeMoco cluster of isolated MoFe protein (Einsle *et al.*, 2002) provides renewed interest for using EXAFS to analyze the structure of FeMoco in the nitrogenase protein. Although, like crystallography, EXAFS cannot distinguish between scatterers of similar atomic number, it would provide a line of structural

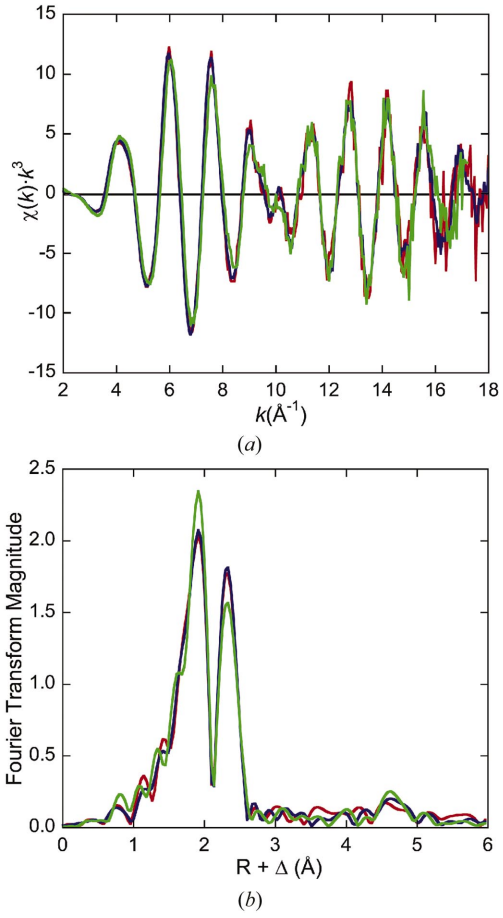

Figure 2
The Mo *K*-edge EXAFS (*a*) and EXAFS Fourier transforms (*b*) for isolated MoFe protein in solution (blue) and single crystal (green), and the ADP·AlF_4^--stabilized nitrogenase complex (red). Note that the MoFe protein crystal data approximate the quality of the solution data even though it represents an average of fewer scans.

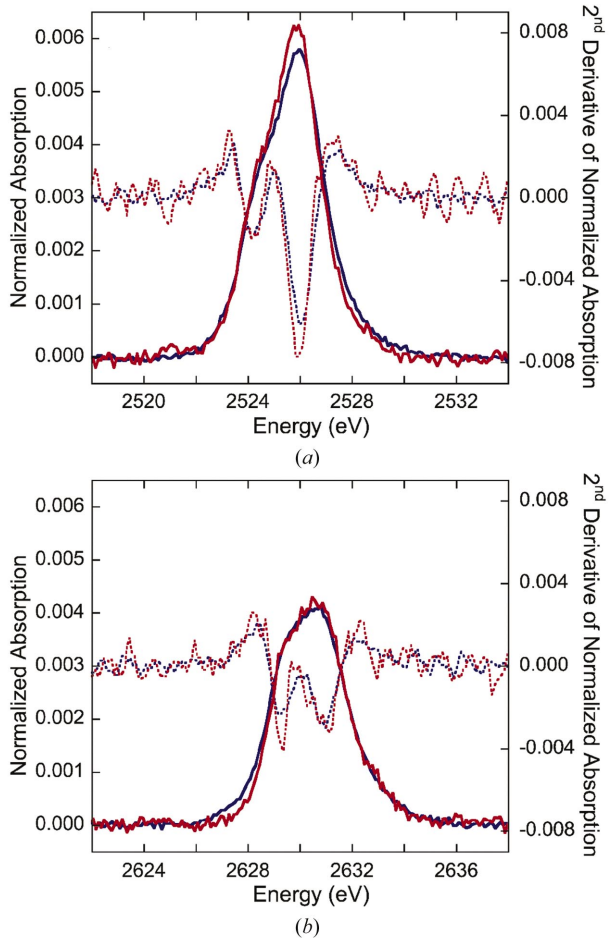

Figure 3
The Mo L_3 (*a*) and L_2 (*b*) edge spectra with smoothed second derivatives (dotted lines) for solution samples of isolated MoFe protein (blue) and the ADP·AlF_4^--stabilized nitrogenase complex (red). The edge spectra cannot be directly overlaid owing to differences in the background absorption, but the second derivatives show good agreement within the noise level of the data.

evidence towards the nature of the interstitial atom. The ability to detect scattering from this atom would rely on Mo–X–Fe multiple scattering along the almost linear cluster axis. This scattering pathway, at approximately 7.0 Å, approaches the distance limit of EXAFS (Rehr & Albers, 2000) and, therefore, would not be resolvable in a typical isotropic solution EXAFS experiment but could likely be detected in a polarized experiment on protein crystals.

Polarized XAS has proven to be a powerful tool, but one that was previously challenging to utilize frequently (Hahn & Hodgson, 1983). In analyzing the absorption edge, polarized XAS allows for a more complete analysis by facilitating the assignment of spectral features, providing specific information about the p_x, p_y and p_z orbitals in some cases, and allowing for unambiguous separation of quadrupole and dipole contributions (Hahn *et al.*, 1982; Smith *et al.*, 1984). For the EXAFS experiment, the angular dependence is included in N^*, the effective polarization-dependent coordination number. At the *K* edge, $N^* = 3N\cos^2\theta$, where θ is defined as the angle between the polarization vector and an absorber-scatter vector (Lee, 1976). Hence, polarization can provide a threefold enhancement of a well aligned feature (Pickering & George, 1995). In

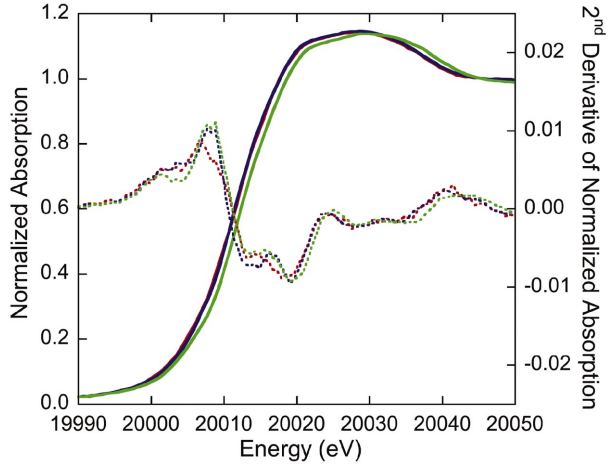

Figure 4
The Mo *K*-edge spectra with smoothed second derivatives (dotted lines) for isolated MoFe protein in solution (blue) and single crystal (green), and the ADP·AlF_4^--stabilized nitrogenase complex (red).

the case of the MoFe protein, spectra collected with the polarization vector aligned parallel and perpendicular to the Mo–X–Fe axis should show either an enhanced or absent signal from the collinear scattering vector. Given adequate data quality, the comparison of these two alignments could provide additional insight as to the position and scattering properties of atom X.

Polarized XAS on MoFe protein crystals has been previously performed (Flank *et al.*, 1986; Chen *et al.*, 1993). However, advances in XAS technology have made it possible to collect data of significantly better resolution, enabling the confident determination of long-range parameters. Further, previous studies relied on mounting pre-oriented crystals, whereas the newly designed single-crystal XAS beamline instrumentation at SSRL, which allows for simultaneous X-ray absorption and diffraction measurements, enables orientation determination, alignment and re-alignment of protein crystals as part of the XAS experiment (Latimer *et al.*, 2005). After a crystal is mounted, its initial orientation can be determined from diffraction data, and then the appropriate positions for XAS measurement can be selected by the Kappa goniometer, which has a large degree of crystal-positioning capability.

Fig. 2 shows an overlay of the EXAFS and EXAFS Fourier transforms from solution and crystal MoFe protein. The data for the crystal represent an average of 20 scans and are as good as, or better than, the average of 31 scans from a protein solution at the upper limit of solution concentration. The overlay of the Mo *K* edges from the solution and single-crystal protein samples in Fig. 4 further highlights the quality of the data that was collected for the single crystal. The slight difference in the edge position is possibly due to polarization effects, the details of which will be pursued in future experiments, or may be due to the difference in the energy resolution of the two beamlines on which data were collected. Table 1 describes the fitting parameters for the single-crystal and solution MoFe proteins. Given the excellent data quality in both the crystal and solution experiments, it is possible to make a one-to-one comparison between these data sets. Although the EXAFS of the crystal do show some polarization effects, especially with respect to E_0 and the low-Z atoms, the distances for the scattering vectors are virtually identical in solution and in the crystal. The crystallographically determined average Mo environment is similar to that found by EXAFS, but with shorter distances for most of the interactions (Einsle *et al.*, 2002). Similar differences in selected distances determined by EXAFS and crystallography have also been established through restrained-refinement approaches to EXAFS analysis (Strange *et al.*, 2003).

In this initial study, XAS data were measured from only one random orientation of the MoFe protein crystal. The polarization vector was determined to be $\sim 60^\circ$ from the FeMoco axis in one half of the MoFe protein dimer and $\sim 45^\circ$ from the other FeMoco axis, for an average polarization angle of $\sim 53^\circ$. Therefore, it is not possible to assess scattering from the interstitial atom at present. The high quality of the data collected from the crystal, both as diffraction (Fig. 5) and XAS, indicate, however, that detecting this atom using the polarized XAS approach and instrumentation is potentially feasible, especially if more scans to a higher *k*-range are measured.

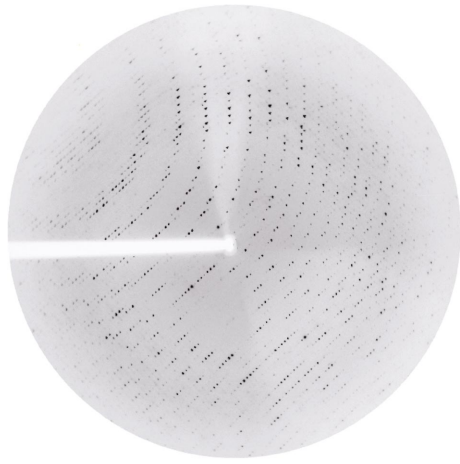

Figure 5
A MarCCD image of the X-ray diffraction at 0.99 Å from the MoFe protein crystal. The image represents a 5 s exposure about a 1° rotation in φ from an approximately cubic crystal measuring ~ 500 µm in each direction.

4. Conclusion

The Mo-*K*- and Mo-*L*-edge XAS edge and *K*-edge EXAFS analyses presented here provide a detailed comparison of isolated MoFe protein in solution with that in a single crystal and with the ADP·AlF_4^--stabilized nitrogenase complex in solution. Our results indicate a lack of perturbation of either the Mo electronic environment or local structure upon nitrogenase complex formation facilitated by ADP·AlF_4^- in agreement with previous findings, but at a more detailed resolution. The double-edge XAS studies on the isolated and complexed MoFe proteins highlight the utility of XAS in studying the nitrogenase system and, more importantly, provide a baseline for future studies on nitrogenase intermediates. Additionally, we show that the FeMoco cluster has the same structure in both a MoFe protein solution and single crystal, which indicates that intermediates generated in either protein solutions or crystals may be compared with the native MoFe protein data presented here. Lastly, our initial study of an oriented MoFe protein crystal using the new SSRL single-crystal XAS capability points to the feasibility of utilizing this technique to determine information about the as yet poorly characterized atom in the center of the FeMoco cluster.

This work was supported by NIH grants RR-01209 (KOH) and GM45162 (DCR). The X-ray data were measured at SSRL, a national user facility operated by Stanford University on behalf of the US Department of Energy, Office of Basic Energy Sciences. The SSRL Structural Molecular Biology Program is supported by the National Institutes of Health, National Center for Research Resources, Biomedical Tech-

nology Program and by the DOE, Office of Biological and Environmental Research.

References

Angove, H. C., Yoo, S. J., Burgess, B. K. & Münck, E. (1997). *J. Am. Chem. Soc.* **119**, 8730–8731.

Burgess, B. K. & Lowe, D. J. (1996). *Chem. Rev.* **96**, 2983–3011.

Chen, J., Christiansen, J., Campobasso, N., Bolin, J. T., Tittsworth, R. C., Hales, B. J., Rehr, J. J. & Cramer, S. P. (1993). *Angew. Chem. Int. Ed.* **32**, 1592–1594.

Christiansen, J., Dean, D. R. & Seefeldt, L. C. (2001). *Annu. Rev. Plant Physiol. Plant Mol. Biol.* **52**, 269–295.

Clarke, T. A., Maritano, S. & Eady, R. R. (2000). *Biochemistry*, **39**, 11434–11440.

Duyvis, M. G., Wassink, H. & Haaker, H. (1996). *FEBS Lett.* **380**, 233–236.

Einsle, O., Tezcan, F. A., Andrade, S. L. A., Schmidt, B., Yoshida, M., Howard, J. B. & Rees, D. C. (2002). *Science*, **297**, 1696–1700.

Ellis, P. J. & Freeman, H. C. (1995). *J. Synchrotron Rad.* **2**, 190–195.

Flank, A. M., Weininger, M., Mortenson, L. E. & Cramer, S. P. (1986). *J. Am. Chem. Soc.* **108**, 1049–1055.

George, G. N. (1990). *EXAFSPAK. Suite of Computer Programs for Analysis of X-ray Absorption Spectra.* Stanford Synchrotron Radiation Laboratory, Stanford, CA, USA.

George, G. N., Cleland, W. E. Jr, Enemark, J. H., Smith, B. E., Kipke, C. A., Roberts, S. A. & Cramer, S. P. (1990). *J. Am. Chem. Soc.* **112**, 2541–2548.

Guo, M., Sulc, F., Ribbe, M. W., Farmer, P. J. & Burgess, B. K. (2002). *J. Am. Chem. Soc.* **124**, 12100–12101.

Hahn, J. E. & Hodgson, K. O. (1983). *Inorganic Chemistry: Toward the 21st Century*, edited by M. H. Chisholm, pp. 431–444. American Chemical Society.

Hahn, J. E., Scott, R. A., Hodgson, K. O., Doniach, S., Desjardins, S. R. & Solomon, E. I. (1982). *Chem. Phys. Lett.* **88**, 595–598.

Hedman, B., Frank, P., Gheller, S. F., Roe, A. L., Newton, W. E. & Hodgson, K. O. (1988). *J. Am. Chem. Soc.* **110**, 3798–3805.

Hedman, B., Penner-Hahn, J. E. & Hodgson, K. O. (1984). *Springer Proc. Phys.* **2**, 64–66.

Howard, J. B. & Rees, D. C. (1996). *Chem. Rev.* **96**, 2965–2982.

Igarashi, R. Y. & Seefeldt, L. C. (2003). *Crit. Rev. Biochem. Mol. Biol.* **38**, 351–384.

Kim, J. & Rees, D. C. (1992). *Science*, **257**, 1677–1682.

Latimer, M. J., Ito, K., McPhillips, S. E. & Hedman, B. (2005). *J. Synchrotron Rad.* **12**, 23–27.

Lee, P. A. (1976). *Phys. Rev. B*, **13**, 5261–5270.

Leslie, A. G. W. (1992). *Joint CCP4 + ESF-EAMCB Newsletter on Protein Crystallography*, No. 26.

Liu, H. I., Filipponi, A., Gavini, N., Burgess, B. K., Hedman, B., Di Cicco, A., Natoli, C. R. & Hodgson, K. O. (1994). *J. Am. Chem. Soc.* **116**, 2418–2423.

Miller, R. W., Eady, R. R., Fairhurst, S. A., Gormal, C. A. & Smith, B. E. (2001). *Eur. J. Biochem.* **268**, 809–818.

Mustre de Leon, J., Rehr, J. J. & Zabinsky, S. I. (1991). *Phys. Rev. B*, **44**, 4146–4156.

Pickering, I. J. & George, G. N. (1995). *Inorg. Chem.* **34**, 3142–3152.

Rehr, J. J. & Albers, R. C. (2000). *Rev. Mod. Phys.* **72**, 621–654.

Renner, K. A. & Howard, J. B. (1996). *Biochemistry*, **35**, 5353–5358.

Schindelin, H., Kisker, C., Schlessman, J. L., Howard, J. B. & Rees, D. C. (1997). *Nature (London)*, **387**, 370–376.

Schmid, B., Einsle, O., Chiu, H.-J., Willing, A., Yoshida, M., Howard, J. B. & Rees, D. C. (2002). *Biochemistry*, **41**, 15557–15565.

Smith, B. E. (1999). *Adv. Inorg. Chem.* **47**, 159–218.

Smith, T. A., Penner-Hahn, J. E., Berding, M. A., Doniach, S. & Hodgson, K. O. (1984). *J. Am. Chem. Soc.* **107**, 5945–5955.

Spee, J. H., Arendsen, A. F., Wassink, H., Marritt, S. J., Hagen, W. R. & Haaker, H. (1998). *FEBS Lett.* **432**, 55–58.

Strange, R. W., Eady, R. R., Lawson, D. & Hasnain, S. S. (2003). *J. Synchrotron Rad.* **10**, 71–75.

Thorneley, R. N. F. & Lowe, D. J. (1983). *Biochem. J.* **215**, 292–403.

Thorneley, R. N. F. & Lowe, D. J. (1985). *Molybdenum Enzymes*, edited by T. G. Spiro, pp. 221–284. New York: Wiley.

Wittinghofer, A. (1997). *Curr. Biol.* **7**, R682–R685.

Wolle, D., Kim, C., Dean, D. R. & Howard, J. B. (1992). *J. Biol. Chem.* **267**, 3667–3673.

Yousafzai, F. K. & Eady, R. R. (1999). *Biochem. J.* **339**, 511–515.